Template synthesis of tubular Sn-based nanostructures for lithium ion storage

Yong WANG[1], Hua Chun ZENG[2] and **Jim Yang LEE**[*,1,2]

[1]Singapore-MIT Alliance, E4-04-10, 4 Engineering Drive 3, Singapore, 117576

[2]Department of Chemical and Biomolecular Engineering, National University of Singapore, Singapore, 119260

Abstract **We report herewith the preparation of SnO$_2$ nanotubes with very good shape and size control, and with and without a carbon nanotube overlayer, The SnO$_2$-core/carbon-shell nanotubes are excellent reversible Li ion storage compounds combining the best features of carbon (cyclability) and SnO$_2$ (capacity) to deliver a high specific capacity (~540-600 mAh/g) simultaneous with good cyclability (0.0375% capacity loss per cycle).**

Index terms **electrochemistry, lithium storage, nanotubes, tin**

I. INTRODUCTION

Sn-based Li storage materials have attracted considerable interest because their storage capacities are more than twice the capacity of graphite. [1-3] The rise to prominence owes a large part to the publicity generated by Fujifilm's announcement,[1] and the numerous scientific investigations which followed thereafter. Their high capacity on both the gravimetric and volumetric basis as well as reasonably low potentials for Li ion insertion and extraction are all very desirable electrochemical properties. There are, however, large specific volume changes in the Li$^+$ insertion and extraction reactions. The internal stress induced by the volume change leads to mechanical failure in the electrode, resulting in poor cycling performance in applications. [1-3]

The mechanical failure may be lessened by rendering the active materials to nanoscale so that the expansion can be made more uniform. A hollow structure in addition will help to provide the free volume needed for the material movement. Hence a pre-organization of zero-dimensional SnO$_2$ nanoparticles into tubular configurations could be a viable solution to the application problem. Concentric expansion and contraction can easily accommodate the tensional stresses imposed, keeping the structural integrity of the tubular configuration. Furthermore, the open tubular structure allows the Li$^+$ ions to diffuse faster into the Sn-based host material through both the external and the internal surfaces of the tube walls, supporting a more symmetric volume expansion and contraction process (benefiting cyclability) and a higher Li storage capacity at a given rate of charge injection and removal.

The preparation of SnO$_2$ nanotubes and the SnO$_2$-carbon tube-in-a tube nanostructure are reported here. An alumina membrane was used to template the growth of cylindrical polycrystalline SnO$_2$ nanotubes within its pores. A uniform CNT overlayer was grown on the external surface of the SnO$_2$ nanotubes through a confined-space catalytic deposition process. When tested for Li storage in the voltage window of 5mV-3V, the SnO$_2$-carbon tube-in-a-tube nanostructure delivered a reversible capacity higher than that of carbon nanotubes (CNTs) with outstanding cyclability. The measured cyclability of 92.5% charge retention after 200 charge and discharge cycles is nearly on par with the performance of commercial graphite anodes.

II. EXPERIMENTAL

Preparation of SnO$_2$ nanotubes in alumina membranes: A porous anodized alumina membrane (Whatman, Anodisc, ϕ = 200 nm) was immersed in water for 30 min under vacuum to remove the air bubble within the pores and then dried before use. SnO$_2$ nanotubes were fabricated by the infiltration of colloidal SnO$_2$ particles into the membrane channels for a number of cycles. In each cycle, the pretreated alumina membrane was placed on a piece of filter paper. SnO$_2$ colloidal suspension (0.1−0.4 ml; 3 wt%) was infiltrated into the membrane under vacuum. The upper surface of the membrane was then polished gently by sand paper (2500 grit). The same procedure was repeated 1 to 8 times. After air drying, the SnO$_2$ encapsulated alumina membrane was calcined in air at 650°C for 10 h. The alumina template was then removed by an aqueous NaOH solution (1.0 M for 10 h or 6.0 M for 30 min). The SnO$_2$ nanotube product was washed with a copious amount of deionized water, followed by centrifuging and drying (5000 rpm; 130°C in a vacuum oven for 3 h).

Preparation of carbon nanotubes in alumina membranes: An Anodisc was placed in a tubular furnace with their pores mounted horizontally. A C$_2$H$_2$ mixture (10% C$_2$H$_2$ and 90% N$_2$, 200 sccm) was passed at 650°C for 3 h before the furnace was cooled naturally in the gas mixture to room temperature.

Preparation of SnO$_2$-carbon composite nanotubes in alumina membranes: An SnO$_2$ nanotube-filled alumina

membrane (prepared from 4 loading cycles) was placed in the tubular furnace with the membrane pores mounted horizontally. A reactive gas mixture (10% C_2H_2 and 90% N_2, 200 sccm) was passed at 650°C for 3 h before the furnace was cooled gradually in the gas mixture to room temperature.

Carbon nanotubes and the SnO_2-core/carbon-shell nanotubes were recovered after the dissolution of the alumina templates by 6M NaOH aqueous solution, followed by generous washing with water, centrifuging at 5000 rpm and vacuum drying at 130°C for 3h. The carbon nanotubes and SnO_2-core/carbon-shell nanotubes were also shortened by intense sonication in 6M NaOH aqueous solution for 30 min. The shortened carbon nanotubes and SnO_2-core/carbon-shell nanotubes were used as the active electrode material for Li storage.

Materials characterizations: The prepared carbon nanotubes, SnO_2 nanotubes and SnO_2-core/carbon-shell nanotubes were characterized by field-emission scanning electron microscopy (FE-SEM), energy dispersive X-ray spectroscopy (FESEM/EDX, JEOL JSM-6700F), transmission electron microscopy (TEM), selected area electron diffraction (TEM/SAED, JEOL JEM-2010F), high-resolution TEM (HRTEM/SAED, Philips FEG-CM300), and powder X-ray diffraction (XRD, Shimadzu XRD-6000, Cu Kα radiation).

Electrochemical measurements: The working electrode was made up of 80 wt% of the active material (Sn-core/carbon-shell nanotubes or carbon nanotubes), 10 wt% of conductivity agent (carbon black, Super-P), and 10 wt% of binder (polyvinylidene difluoride, PVDF, Aldrich). Lithium foil was used as the counter electrode, and electrolyte was 1 M $LiPF_6$ in a 50:50 w/w mixture of ethylene carbonate (EC) and diethyl carbonate (DEC). Cell assembly was carried out in a recirculating argon glove box with moisture and oxygen contents below 1ppm each. All cells were tested galvanostatically at the ~0.5 C rate (0.3 mA/cm^2 or 340 mA/g for SnO_2-core/carbon-shell anode; 0.13 mA/cm^2 or 180 mA/g for carbon nanotubes) and were charged (Li$^+$ insertion) and discharged (Li$^+$ extraction) between fixed voltage limits (3 V-5mV).

III. Results and discussion

Figure 1 shows the morphology of the SnO_2 nanotubes. The nanotubes (obtained with 8 loading cycles) after the removal of the alumina template were recovered in the form of bundles. The nanotubes were quite uniform with diameters in the range of ~180−230 nm (Figure 1b and c), which varied little from the denoted pore size (200 nm) of the membrane. A top view of the nanotubes is provided in Figure 1d. The open tubular nanostructures were well aligned, and the cross-sections of the nanotubes were indeed circular. Analysis with energy-dispersive X-ray spectroscopy (EDX) revealed that the Sn:O ratio was 1:2, confirming the stoichiometry of the product as SnO_2. In addition, all the peaks in the powder X-ray diffraction (XRD) pattern of the

product (Figure 2a) could be indexed to the rutilelike SnO_2 with tetragonal lattice constants ao = 4.74 Å and co = 3.19 Å
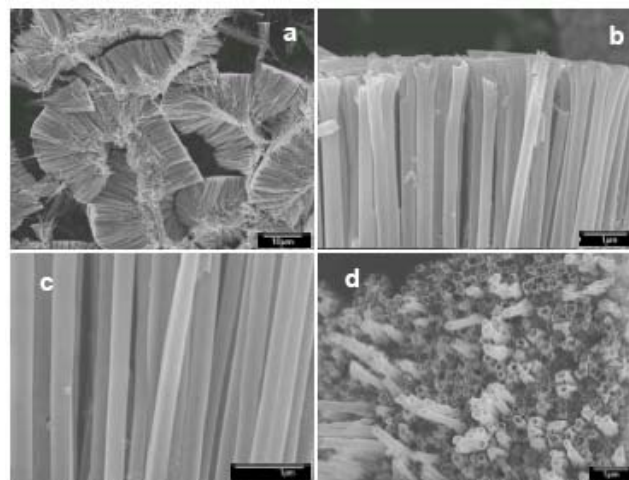

Fig. 1. FESEM images of the SnO_2 nanotubes prepared by infiltration after 8 cycles: a) Large assemblies of as-prepared nanotubes. b) Side-view of top section. c) Side-view of body section. d) Top-view of nanotubes.
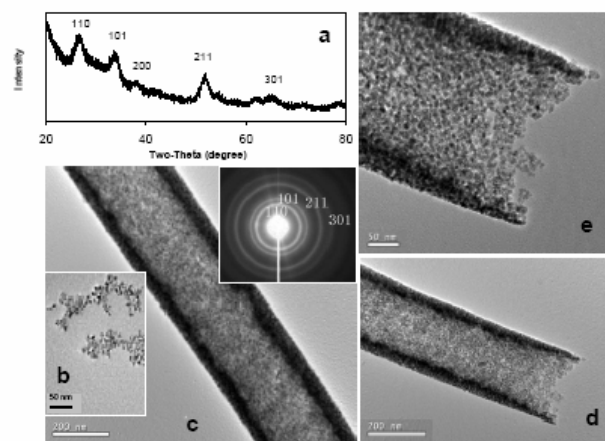

Fig. 2. a) The XRD pattern of SnO_2 nanotubes prepared after 8 cycles of infiltration. b) TEM image of the primitive SnO_2 nanoparticles. c) TEM images of an individual SnO_2 nanotube prepared after 8 cycles of infiltration (inset is its corresponding SAED pattern). d) & e) The open end of the same nanotube in c) at different magnifications.
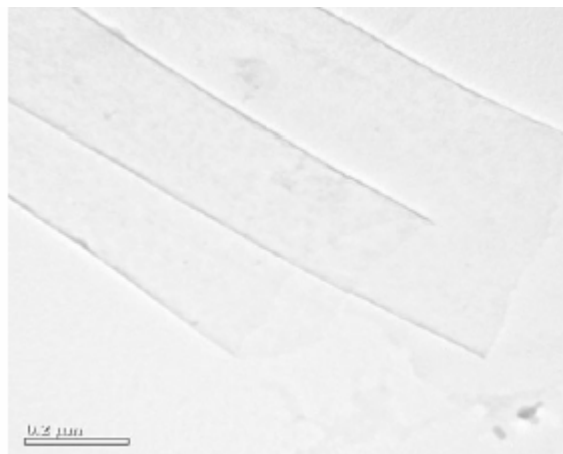

Fig. 3. TEM image of open-ended carbon nanotubes (CNTs)

(JCPDS 41-1445). The colloidal SnO_2 nanoparticles which were used as the starting building blocks of SnO_2 nanotubes were examined by transmission electron microscopy (TEM). Figure 2b shows that the particles were slightly agglomerated with sizes in the range of ~6−15 nm (The denoted particle size was 10−15 nm). TEM investigation indicated no appreciable particle growth after the thermal treatment at 650°C, although the crystallinity of the material was improved. The rutile phase of SnO_2 is also confirmed by the selected area electron diffraction (SAED) pattern in the Figure inset. Interestingly, even with a higher number of infiltrations, the porous nature of the nanotube-walls was still observed. It is believed that the intra-wall space created by the wall porosity not only provides additional routes for Li^+ transport/insertion but also enhances the dimensional stability of the nanotubes to withstand a larger extent of volume change in the charging-discharging cycles. In addition to the control of wall-thickness, the length of SnO_2 nanotubes could also be tailored. Using a higher concentration NaOH solution (6.0 M) to remove the alumina template, followed by 5 min of sonication, the as-prepared nanotubes were significantly shortened compared to the use of 1.0 M NaOH. The shortened nanotubes had more openings to substantially reduce the diffusion paths of Li^+ ions into the internal surface. Quite surprisingly, the bundle-like arrays prevalent in the longer nanotubes (Figure 1) were not present in the shorter nanotubes. These non-aggregated nanotubes could allow a more intimate blending with the conductivity agent and the binder and prevent inter-tube agglomeration.

Commercial alumina membranes with denoted pore size of 200 nm could be used to form CNTs with the same diameter via the thermal decomposition of C_2H_2 (Figure 3). The alumina walls served well as the catalyst needed for the CNT deposition.[4] On the other hand, porous SnO_2 nanotubes could also be formed inside the alumina pores using the same infiltration technique. Figs.4a,b are respectively the FE-SEM and TEM images of the SnO_2 nanotubes after 4 loading cycles using the 3 wt% commercial SnO_2 colloidal solution (10-15 nm nominal). The SnO_2 nanotubes had uniform diameters (~200 nm) and the tube walls were again made up of many small nanoparticles ~10 nm in size. The SnO_2-filled alumina templates were the starting material for the fabrication of SnO_2-core/carbon-shell tubular nanostructures. Fig. 4c,d show two FE-SEM side-views of the final product from the pyrolysis of C_2H_2 inside the SnO_2-filled alumina templates. All of the nanotubes in the flexible tube bundle had very smooth outer walls similar to those of CNTs. Energy-dispersive X-ray spectroscopy (EDX) indicated the presence of large quantities of C, Sn, and O elements in the mole ratio of ~ 7:1:2. The tubes were open-ended with circular faces as can be seen in the FE-SEM top-views in Figure 5a, 5b. The high magnification FE-SEM image in Fig. 5b also shows a few remnant nanoparticle on the inside of the tubular walls. A few ruptured nanotubes were captured in Figs. 5c, 5d showing a roughened and highly textured internal wall which contrasts strongly with the smooth and
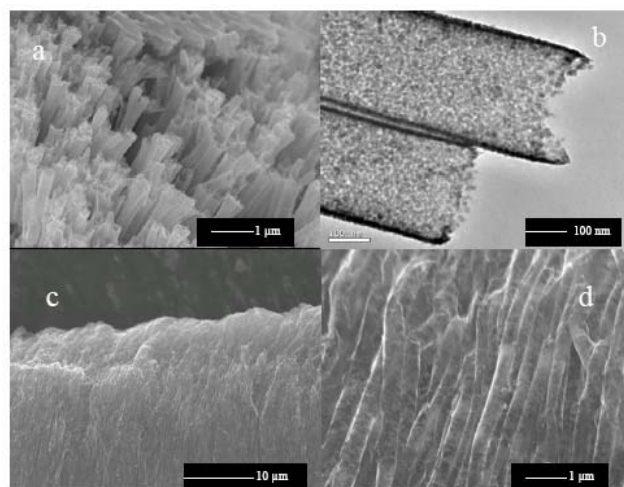

Fig. 4 SnO_2 nanotubes prepared from commercial SnO_2 nanoparticles by a 4-cycle template infusion technique: a) FE-SEM image, b) TEM image. SnO2-core/carbon-shell nanotubes: c) low magnification FE-SEM side view, and d) high magnification FE-SEM side view.
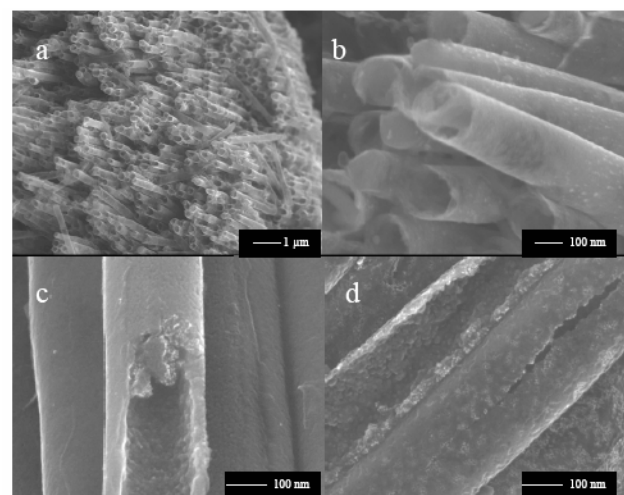

Fig. 5 FE-SEM images of SnO_2-core/carbon-shell nanotubes a) top view, b) top view, and c,d) ruptured SnO_2-core/carbon-shell nanotubes.
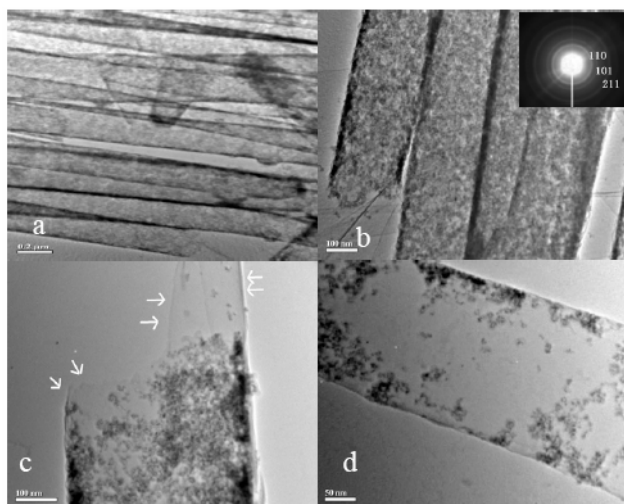

Fig. 6 TEM images of a-b) a few oriented SnO_2-core/carbon-shell nanotubes, c) the tip of an isolated SnO_2-core/carbon-shell nanotube showing the CNT overlayer, and d) an incompletely formed core-shell structure showing a few random SnO_2 nanoparticles inside the carbon nanotubes. The inset of b) shows the corresponding SAED pattern.

nearly featureless external wall. TEM examination confirmed the SnO_2-core/carbon-shell tubular structure, showing a large number of open-ended nanotubes with the same diameter (~200 nm) and uniform arrangement of nanoparticles on the inside walls (Figures 6a,b). The corresponding selected area electron diffraction (SAED) consisted of a few diffraction rings consistent with the Powder XRD patterns of rutile structure of tin oxide. All the diffraction peaks in Figure 7 can be indexed to rutile-like SnO_2 with tetragonal lattice constants a_o= 4.74 Å and c_o = 3.19 Å (JCPDS 41-1445). It should be noted that the (002) diffraction of graphite, if present, would be over-shadowed by the (110) reflection of SnO_2 at nearly the same position. There are also a few weak reflection peaks from Sn, indicating that some SnO_2 was reduced by C_2H_2 during the template deposition of CNTs.

The tip of an isolated composite nanotube is shown in the TEM image of Fig. 6c, where the arrows highlight the carbon skin around the broken edge of the tube. The thickness of the carbon skin was ~4 nm, making it difficult to be differentiated from the SnO_2 nanotubular core other than at the broken edge. HRTEM analysis of the ~ 4nm carbon skin showed a multiwalled CNT structure with an interplanar distance of ~0.35 nm (Fig. 8).

The inner SnO_2 nanotubes were formed by the ordered alignment of SnO_2 nanoparticles. For comparison, an alumina template treated with only one loading cycle of SnO_2 nanoparticles was also used to fabricate SnO_2-core/carbon-shell nanocomposites. For this sample the number of SnO_2 nanoparticles was insufficient to form a contiguous wall, and discrete particles could be found to distribute randomly on the inside of the ~200 nm CNTs (Fig. 6d).

Based on the FE-SEM, TEM, and HRTEM observations, it is believed that C_2H_2 diffused through the porous SnO_2 nanotubes and was decomposed to CNT in the annular space between the SnO_2 nanotubes and the walls of the alumina pores, by the catalytic action of the latter. A tightly integrated SnO_2-core/carbon-shell nanostructure was formed as a result. The completely stratified core-shell structure was well-grown with uniform shape and size; with 100% coverage of the SnO_2 surface by CNT. A reversal in the deposition sequence, i.e. using CNT formation as the first step, was unable to produce the core-shell nanostructured product. The infiltration of SnO_2 nanoparticles into the AAO pores constricted by pre-deposited CNT was extremely difficult, and most SnO_2 nanoparticles would accumulate at the pore mouths. The sequential templated growth technique demonstrated here can in principle be extended to other metals and metal oxides to form tubular nanostructures with coaxially grown CNT overlayers.

The SnO_2-core/carbon-shell nanotubes were found to contain 73.3wt% SnO_2 as determined by inductively coupled plasma (ICP) spectroscopy. Before the electrochemical tests, the core-shell nanotubes were shortened in a NaOH aqueous solution. The shortened core-
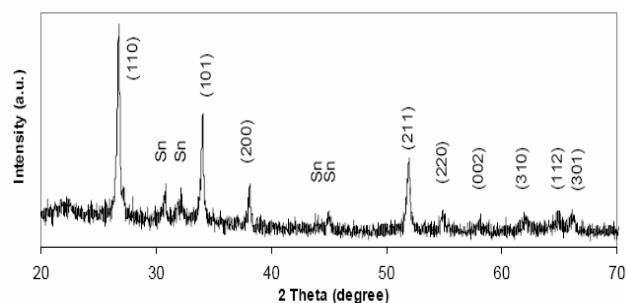

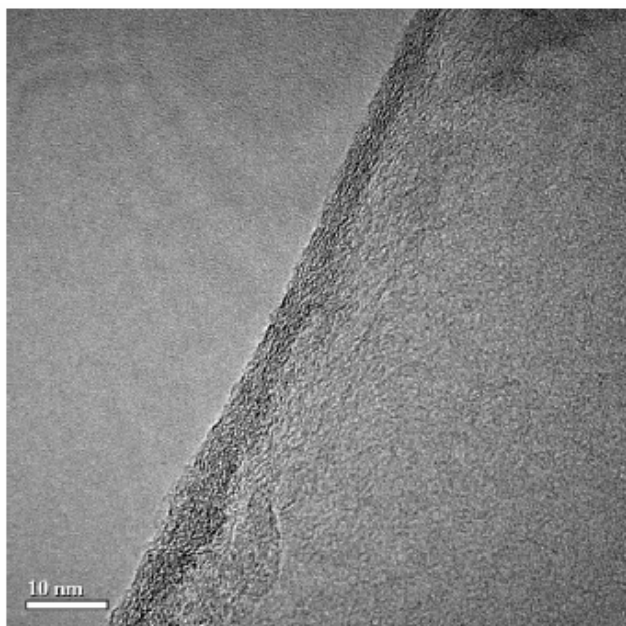Fig. 7 Powder XRD patterns of SnO_2-core/carbon-shell nanotubes

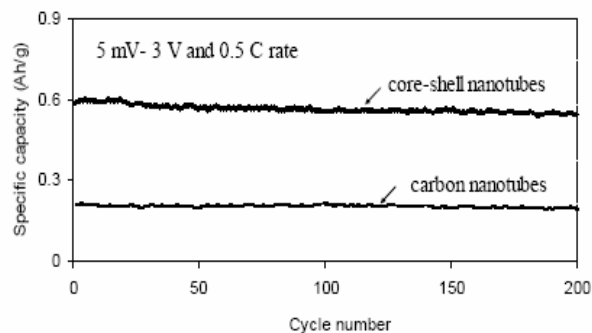Fig. 8 HRTEM image of the edges of a multiwalled carbon nanotube shell.

Fig. 9 Cycling performance of SnO_2-core/carbon-shell nanotubes and carbon nanotubes in the 5 mV- 3 V (vs. Li$^+$/Li) voltage window, and ~0.5 C.

shell nanotubes and the resulting decrease in Li diffusion pathways should benefit lithium ion transport. The cycling

performance of SnO$_2$-core/carbon-shell nanotubes was measured at a constant current density of 0.3 mA/cm^2 (~0.5 C) over the voltage window of 5 mV – 3 V, where substantial capacity fading is often observed for Sn-based Li storage compounds.[1-3] Fig. 5 shows the cycling performance of the SnO$_2$-core/carbon-shell nanotube anode. At the relatively high charge and discharge current of ~0.5 C, the core-shell nanotube anode could be repeatedly charged and discharged for 200 cycles with good cyclability. The initial specific capacity of ~586 mAh/g was reduced to 542 mAh/g, or 92.5% of the initial capacity, after 200 cycles. The capacity fade rate was only 0.0375% per cycle, which places it on par with the performance of commercial graphite-based anodes (~0.03% per cycle). To the best of our knowledge, such stable performance under a relatively high rate of charge and discharge (0.5 C), and in voltage windows with a cut-off voltage above 1.5 V, is unprecedented for a SnO$_2$-based Li storage compound. Compared to CNT anodes which often display reversible specific capacities not exceeding ~200 mAh/g, the specific capacity of the SnO$_2$-core/carbon-shell nanotube anode reflects a sizeable 3-fold increase (Figure 9). The volumetric capacity and the energy density should likewise be higher because the void space of CNTs is now filled with a high capacity Li storage compound.

In general, when charging to V>~0.9 V, Sn-based anodes often display very poor cyclability (~3% capacity loss per cycle compared to ~0.03% capacity loss per cycle for graphite). The capacity loss is believed to be caused by stress-induced material failure arising from the volume change in charging (Li-Sn alloying) and discharging (Li-Sn dealloying) reactions, which scales with the particle size of the Sn active phase. The common countermeasures include a more restricted operational window (with cut off voltage <0.9 V), [1-3] or the dispersion of Sn or SnO$_2$ as small particles in a stress-absorbing soft matrix. [5-6] For example carbonaceous materials have been used to extend the cyclability of SnO$_2$ successfully. In this work, a CNT skin and a tubular organization of SnO$_2$ nanoparticles were used to relieve the stress induced by cycling. The TEM and FE-SEM (not shown) examination of the core-shell nanotube anode after 200 cycles of charging and discharging confirmed that the tubular geometry was intact and that the ~10-15 nm tin nanoparticles constituting the SnO$_2$ nanotubes were still detectable on the inside surface of the duplex nanotubes. There was therefore no significant particle growth with cycling. The limited particle growth and the good cycling performance may be attributed to the following factors: A tubular organization of SnO$_2$ nanoparticles limits the mobility of particles during cycling. The flexible CNT skin further improves the stability of tin oxide particles against agglomeration, resulting in an excellent cyclability. The large internal void in the core-shell construction buffers well against the local volume change in Li-Sn alloying and de-alloying reactions. The good electrical conductivity of CNTs is useful to keeping the SnO$_2$ nanoparticles electrically connected during all stages of charge and discharge. The porosity in the SnO$_2$ nanotubes and the large surface areas[5-6] available from both the interior and exterior of the core-shell nanotubes also contribute positively to lithium ion diffusion. The successful use of a tubular core-shell nanostructure to address the rapid capacity fading of SnO$_2$ anodes is inspiring to overcoming similar problems in other Li-alloying elements such as Si and Sb.

IV. CONCLUSION

In summary, uniform polycrystalline SnO$_2$ nanotubes (in array or freestanding form) can be fabricated by an infiltration technique using SnO$_2$ nanoparticles as the building blocks. The diameter, length, thickness, and texture of the nanotubes can be controlled. A new SnO$_2$-C composite structure, namely porous SnO$_2$ nanotubes with coaxially grown CNT overlayers was also obtained by a two-step sequential template deposition method. Quite unlike the common approach of infiltrating the CNT void space with a filler material (which can hardly be done at 100% filling rate, especially for CNTs with small diameters), the new method made use of confined-space deposition to form a uniform CNT skin over preformed porous SnO$_2$ nanotubes. The SnO$_2$-C nanocomposite exhibited high reversible capacity (~540-600 mAh/g) and excellent cyclability (0.0375% capacity loss per cycle, comparable to the performance of commercial graphite) in Li ion storage and retrieval, making it suitable as an active anode material for lithium-ion batteries. The outstanding electrochemical properties are likely to be related to several unique features of this nanocomposite: tubular organization of tin oxide nanoparticles, stress absorption by the CNT matrix, and the existence of a hollow interior allowing freedom of expansion, increased electrical contact, and enhanced lithium ion transport.

REFERENCES

[1] Y. Idota, A. Matsufuji, Y. Mackawa, and T. Miyasaki, "Tin-based amorphous oxide: A high-capacity lithium-ion-storage material," *Science,* vol. 276, pp.1395-1397, 1997.

[2] M. Winter and J. O. Besenhard, "Electrochemical lithiation of tin and tin-based intermetallics and composites," *Electrochim. Acta*, vol. 45, pp.31-50, 1999.

[3] M. Winter, J. O. Besenhard, M. E. Spahr and P. Novak, "Insertion electrode materials for rechargeable lithium batteries," *Adv. Mater.* vol. 10, pp. 725-763,1998.

[4] Y. C. Sui, B. Z. Cui, R. Guardian, D. R. Acosta, L. Martinez and R. Perez, "Growth of carbon nanotubes and nanofibres in porous anodic alumina film," *Carbon*, vol. 40, pp.1011-1016, 2002.

[5] E. Kim, D. Son, T. G. Kim, J. Cho, B. Park, K. S. Ryu and S. H. Chang, "A mesoporous/crystalline composite material containing tin phosphate for use as the anode in lithium ion batteries," *Angew. Chem. Int. Ed.* Vol. 43, pp. 5987-5990, 2004.

[6] J. Fan, T. Wang, C. Yu, B. Tu, Z. Jiang and D. Zhao, "Ordered, nanostructured tin-based oxides/carbon composites as the negative-electrode material for lithium ion batteries," *Adv. Mater.* Vol. 16, pp.1432-1436, 2004.